Structural, Optical and Magnetic Feature of Core-Shell Nanostructured Fe_3O_4@GO in Photocatalytic Activity

Abharya, Amir; Gholizadeh, Ahmad*[+]

School of Physics, Damghan University (DU), Damghan, I.R. Iran

ABSTRACT: *In this paper, structural, magnetic, optical, and photocatalytic properties of core-shell structure Fe_3O_4@GO nanoparticles have been compared with Fe_3O_4 nanoparticles in the degradation of methyl blue and methyl orange. For this purpose, GO nanosheets were wrapped around the APTMS-Fe_3O_4 nanoparticles and then characterized using X-ray Diffraction, field emission scanning electron microscopy, transmission electron microscopy, vibrating sample magnetometer, UV-visible, and Fourier transform infrared spectroscopy. The results show the core-shell nanostructured Fe_3O_4@GO is formed. As an application for the synthesized structure, degradation of methyl blue and methyl orange as heavy-mass organic pollutants has been measured. While the saturation magnetization of Fe_3O_4@GO is lower than Fe_3O_4, but shows better efficiency in the degradation of methyl blue and methyl orange. The obtained catalysts can be quickly separated from the solution under an external magnetic field because of their considerable Ms values, which will be beneficial for their reuse and boosting the overall water treatment efficiency in practical applications.*

KEYWORDS: *Graphene oxide; Core-shell structure; Magnetic materials; Degradation of methyl blue and methyl orange.*

INTRODUCTION

The synthesis of transition metals and their oxide NanoParticles (NPs) is of importance in nanotechnology research due to their potential and practical applications [1]. Among the materials, the oldest known ferrite, Fe_3O_4, has raised much interest in the field of information storage as well as the areas of biomedicine and magnetic sensing. In recent years, magnetic nanoparticles have attracted much attention because of their unique properties and various applications [1-3]. They are biocompatibility which enables them for applications in developing magneto-electronic and spin-valve devices and in various biomedical applications [4].

Graphene, a 2D, the sp2-hybridized hexagonal lattice of carbon atoms, is a material that has attracted significant attention because of its unusual electronic structure, excellent electrical, thermal, optical, and mechanical properties, and possible technological applications [5-6]. The difference in the structure of GO and graphene lies in a large amount of chemical functional groups attached to the carbon plane and structural defects within the plane, both of which can severely decrease the electrical conductivity [5]. The reduction of Graphene Oxide (GO) can be considered to be aimed at achieving two targets: the elimination

***** *To whom correspondence should be addressed.*

+ E-mail: gholizadeh@du.ac.ir

1021-9986/2020/2/49-58 10/$/6.00

of functional groups and the healing of structural defects. Although graphene is hard to manufacture but GO that can be easily synthesized by physical and chemical methods, instead of graphene can be used in different technology applications [6].

Composites with a magnetic core and functional shell structures have received special attention because of their potential applications in catalysis, selective separation, chromatography, chemical or biologic sensors, yielding also multiple function systems. Generally, according to the literature, the interactions between different components can improve the performance of the multi-components system and even generate new synergetic properties [7]. Due to their combined optical and magnetic properties, core-shell magnetic nanostructures can provide new applications in biotechnologies, in bio-separation, bio-imaging, targeted drug delivery, tumor cell localization, hyperthermia, and even malignant cells destruction.

Regarding the catalytic applications of core-shell composites, new processes appear at the interface between the nanostructured catalyst and the supporting material. Thus, ferroelectric nanoparticles may produce an electric polarization at the interface with active catalytic nanoparticles. On the other hand, magnetic systems are ease to be conveniently collected, separated, or fixed by an external magnet. Moreover, charge and spin transfer occurs at the interface between the magnetic component and its catalytic active companion, adjusting catalytic properties [7-8].

Wei et al. [8] prepared core–shell structure Fe_3O_4@graphene oxide (GO) submicron particles have been prepared via a simple electrostatic self-assembly process for use in adsorption of bovine serum albumin as a model protein. The results showed that performance of GO as a shell material for core–shell magnetic composites was found to be superior to that of conventional shell materials such as polymers and silicon, thus demonstrating the great potential of the Fe_3O_4@GO particles for application in magnetic bio-separation. A reclaimable Fe_3O_4/graphene oxide (GO) superparamagnetic hybrid was successfully synthesized via a facile one-pot polyol approach and employed as a recyclable adsorbent for Bisphenol A (BPA) in aqueous solutions [9]. The results indicated that the Fe_3O_4/GO hybrid could be regarded as a potential adsorbent for wastewater treatment and purification processes. *He et al.* [10], attached the Fe_3O_4 nanoparticles to graphene oxide by covalent bonding. The attachment of Fe_3O_4 NPs on the GO nanosheet surface was confirmed by transmission electron microscopy and Fourier-transform infrared spectroscopy. The adsorption capacity of GO– Fe_3O_4 for methylene blue and neutral red cationic dyes was as high as 190.14 and 140.79 mg/g, respectively. *Li et al.* [11], developed a new and relatively general route to fabricate Graphene Oxide (GO)– Fe_3O_4 hybrid. This hybrid shows superparamagnetic property and allows the rapid separation under an external-magnetic field. Degradation of phenol using Fe_3O_4-GO nanocomposite as a heterogeneous photo-Fenton catalyst showed that under optimal conditions with UV-light irradiation, about 98.8% phenol and 81.3% TOC of a phenol solution could be removed after 120 min photo-Fenton degradation [12]. It can be seen that UV-light improves significantly the phenol removal in the photo-Fenton process. The introduction of GO in the catalyst promotes the photo-Fenton reaction via three roles: increasing adsorption capacity, offering more active sites and accelerating the Fe^{3+}/Fe^{2+} cycle under UV light irradiation. It was also observed that Fe_3O_4-GO still showed high catalytic activity after five cycles.

Nowadays, regulation on the discharge of dye-polluted colored wastewater has been getting stringent in many countries [13]. The presence of even small amounts of dyes in water, less than 1 ppm for some dyes, is highly visible and undesirable. It is estimated that more than 100,000 commercially available dyes with over 7×10^5 tons of dyestuff are produced annually. Therefore, many publications try to offer various catalysts for improving the efficiency of the reaction, among them metal oxides are known as a heterogeneous catalyst [14]. In this work, we report the synthesis of a novel type of core-shell structured Fe_3O_4@GO nanoparticles by a simple self-assembly process. The process is driven by the mutual electrostatic interaction between negatively charged GO sheets and positively charged APTMS modified Fe_3O_4 particles, which resulted in a flexible and ultrathin GO coating enwrapping the Fe_3O_4 particles. Fe_3O_4 nanoparticles prepared by co-precipitation method were employed in an attempt to give a material with high saturation magnetization. Fig. 1 show the chemical structure of Methyl Blue (MB, $C_{37}H_{27}N_3Na_2S_3O_9$) and

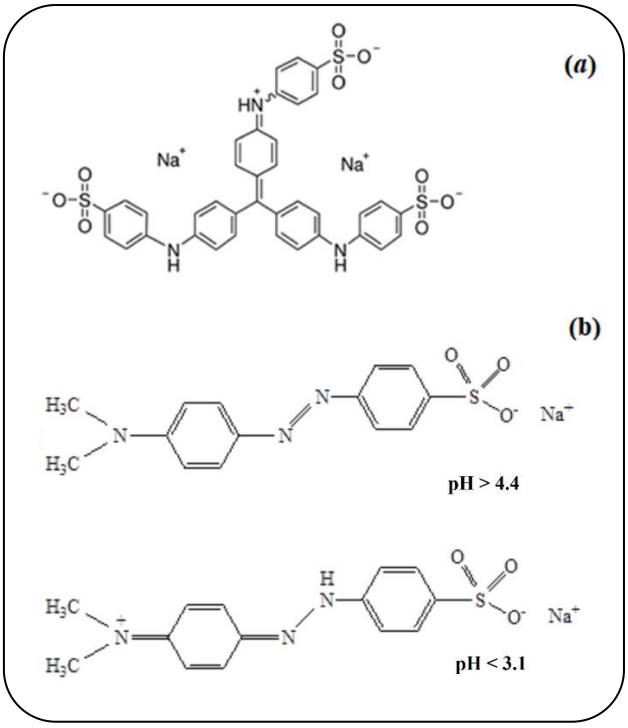

Fig. 1: Chemical structure of (a) methyl blue dye and (b) methyl orange dye in PH ≥ 4.4 and PH ≤ 3.1.

methyl orange (MO, $C_{14}H_{14}N_3NaO_3S$) as a kind of dye. It is expected that the synergistic effect between adsorption and catalysis will significantly promote the decolonization of Methyl blue and methyl orange from wastewater by chemical oxidation method under ambient sunlight and natural pH.

EXPERIMENTAL SECTION

Materials

Synthesis of Fe_3O_4

The Fe_3O_4-NPs were prepared according to the following method [1]. $FeCl_2{\cdot}4H_2O$ (2.0 g, 0.01 mol.) and $FeCl_3{\cdot}6H_2O$ (5.4 g,0.02 mol.) were dissolved in 120 mL deionized water, and then, 60 mL $NH_3{\cdot}H_2O$ was added under vigorous mechanical stirring. The color of the suspension turned black immediately. Afterward, the mixture was kept at 70°C for 30 min. The mechanical stirring was carried out throughout the reaction. After cooling down, the precipitated powders were collected by magnetic separation and washed with deionized water.

Synthesis of GO

For the improved method [15], a 9:1 mixture of concentrated H_2SO_4/H_3PO_4 (360:40 mL) was added to a mixture of graphite flakes (3.0 g, 1 wt. equiv.) and $KMnO_4$ (18.0 g, 6 wt. equiv.), producing a slight exotherm to 35-40 °C. The reaction was then heated to 50 °C and stirred for 12 h. The reaction was cooled to RT and poured onto ice (400 mL) with 30% H_2O_2 (3 mL). The solution was centrifuged (4000 rpm for 4 h), and the supernatant was decanted away. The remaining solid material was then washed in succession with 200 mL of water, 200 mL of 30% HCl, and 200 mL of ethanol (2 times); for each wash, the mixture was sifted through the U.S. Standard testing sieve and then filtered through polyester fiber with the filtrate being centrifuged (4000 rpm for 4 h), and the supernatant decanted away. The material remaining after this extended, was vacuum-dried overnight at room temperature, obtaining 5.8 g of product.

Synthesis of Fe3O4@GO

0.5 g of the obtained Fe_3O_4 was homogeneously dispersed in isopropyl alcohol solution by ultrasonic for 30 min [7]. Afterward, 0.5 mL of 3-Aminopropyltrimethoxysilane (APTMS) molecules were added to the above mixture and refluxed at 80 °C for 24 h. The products were washing by ethanol several times and then dried in a vacuum oven. Finally, 100 mL homogeneous aqueous solution of the APTMS modified Fe_3O_4 (APTMS- Fe_3O_4) was mixed with 150 mL of 0.5 mg/mL GO for about 30 min under mechanical stirring to get GO wrapped Fe_3O_4 (Fe_3O_4@GO) nano-spheres.

Characterization

The X-ray diffraction (XRD) pattern of the samples was obtained using a Bruker X-ray diffractometer (Bruker-AXS, Karlsruhe, Germany) with Cu-Kα radiation (λ = 1.54048 Å) source over an angle range of 2θ = 5-75° and a resolution of 0.02. Scherrer's equation indicates the broadening of the XRD pattern which is attributed to the crystallite size-induced broadening [16]:

$$D = \frac{0.94\lambda}{\beta_{hkl}\cos\theta} \quad (1)$$

Here, β_{hkl} is the full-width at half-maximum of the diffraction peak (311) located at about 2θ = 35˚. Generally, the relationship between the inter-planar spacing d of the plane with miller's indices (hkl) for cubic system and Bragg condition is given by the following form:

$$\frac{4\sin^2\theta}{\lambda^2}=\frac{1}{d^2}=\frac{h^2+k^2+l^2}{a^2} \quad (2)$$

Where *a*, and *c* are the lattice parameters and, θ and λ are the Bragg angle and incident X-ray wavelength. For all samples, lattice parameter *a* was calculated from the position of the (311) diffraction peak and Eq. (2).

The Fourier Transform InfraRed (FT-IR) spectra of samples were recorded by using a Perkin-Elmer FT-IR spectrometer in the wave number range from 350 cm^{-1} to 2000 cm^{-1}. The dried samples were blended with a ratio of 1 to 100 with KBr powder and before spectrum acquisition were pressed into tablets. Surface morphology images of the samples were analyzed by field emission scanning electron microscopy (FE-SEM, HITACHI S-4160 model). The particle size of the samples was investigated by the transmission electron microscopy (TEM, LEO Model 912AB) analysis. The hysteresis loops at room temperature were carried out in a vibrating sample magnetometer (VSM, 7400 Lake Shore). The value of saturation magnetization of the samples has been calculated by the law of approach to saturation [17]. The band gap energy of the samples was estimated through the optical absorption spectra recorded between 200 and 1100 nm wavelengths with a UV-Vis system (Agilent8453, Palo Alto, CA). The relation between the optical absorption coefficient, α (λ), and the optical gap energy (E_g) of a direct transition according to the Tauc's equation [18, 19]:

$$(\alpha h\nu)^2 = B(h\nu - E) \quad (3)$$

Where, B is an energy-independent constant and $\alpha(\lambda)=2.303A(\lambda)/t$ is the optical absorption coefficient where $A(\lambda)$ and t represent the absorption spectra and the mean particle size of the sample, respectively. The band gap energy of the samples is estimated by extrapolating the linear part of $(\alpha h\nu)^2$ versus the $h\nu$ plot.

Then, the photocatalytic activity of nanoparticles for degradation of methyl blue and methyl orange aqueous solutions is investigated using absorption spectra at wavelengths range of 300-700 nm. Before lighting, the suspension is sufficiently stirred for 20 min to reach adsorption-desorption equilibrium between the catalysts and methyl blue so that the adsorption in the without catalyst can be discounted. The effect of the absorbent and contact time are studied to obtain optimal conditions.

RESULTS AND DISCUSSION

Structural and morphology properties

X-ray diffraction patterns of the samples are shown in Fig. 2. Moreover, the diffraction peak of GO is observed at about 2θ = 10.1°, in agreement with typical graphene oxide feature [8]. The XRD pattern of Fe_3O_4@GO is very similar to that of the pristine Fe_3O_4, with diffraction peaks which can be indexed as the characteristic (200), (311), (400), (422), (511) and (440) reflections of the pure cubic spinel crystal structure of Fe_3O_4 (JCPDS no. 19-0629) [1]. However, the characteristic 002 diffraction peak of GO was not observed in the XRD pattern of the Fe_3O_4@GO, although it was observed in the diffraction pattern of the GO precursor. This indicates that GO was enwrapped uniformly around the Fe_3O_4 particles.

The values of the lattice parameter (*a*) for Fe_3O_4 and Fe_3O_4@GO are 8.368 and 8.364 Å, respectively. The decrease of the lattice constant can be attributed to an increase in the presence of Fe^{3+}-ions on B-site of Fe_3O_4@GO in compared with Fe_3O_4 [1]. Also, the values of the crystallite sizes for Fe_3O_4 and Fe_3O_4@GO are 9.61 and 9.40 nm, respectively. The decrease of the crystallite sizes of the samples has been attributed to the decrease of the lattice parameter in samples [20].

Fig. 3 shows the FT-IR spectra of Fe_3O_4, GO and Fe_3O_4@GO. The positions of two strong bands υ_1 and υ_2 about 574 cm^{-1} and 430 cm^{-1} in FTIR spectra of Fe_3O_4 are related to spinel cubic structure. The band υ_1 is assigned to the vibrations of the bond between the tetrahedral metal ion and the oxygen ion M_{tetra}–O. Also, the band υ_2 is assigned to the vibrations of the bond between the octahedral metal ion and the oxygen ion M_{octa}–O [4]. Therefore, the formation of spinel structure has also been confirmed by FTIR measurement as obtained from XRD result. The functional groups are also identified in FT-IR spectra of the samples as follow [21]: the absorption band at 3450 cm^{-1} was owing to the stretching vibrations of the hydroxyl group (OH) due to the presence of acid or water in the samples; the adsorption band at approximately 1545 cm^{-1} corresponds to the C=C bonding of aromatic rings; the carboxyl (COOH) stretching vibration peak at 1720 cm^{-1} in the carbonyl group, and also 1052 cm^{-1} and 1160 cm^{-1} are due to aromatic anti-symmetrical coupled stretching of C-O and C-C bonding, respectively. Two peaks assigned to the hydroxyl group and attached

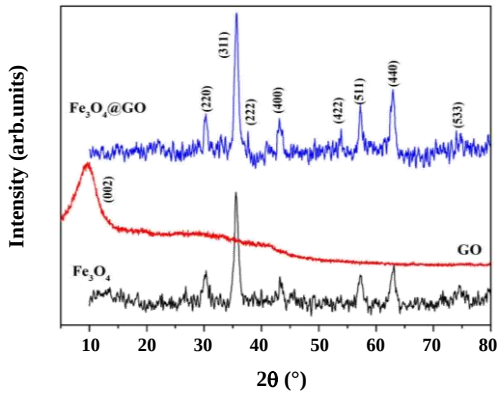

Fig. 2: XRD patterns of Fe_3O_4, GO, and Fe_3O_4@GO.

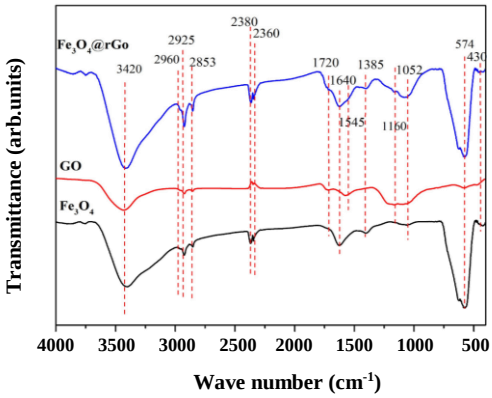

Fig. 3: FT-IR spectra of Fe_3O_4, GO, and Fe_3O_4@GO.

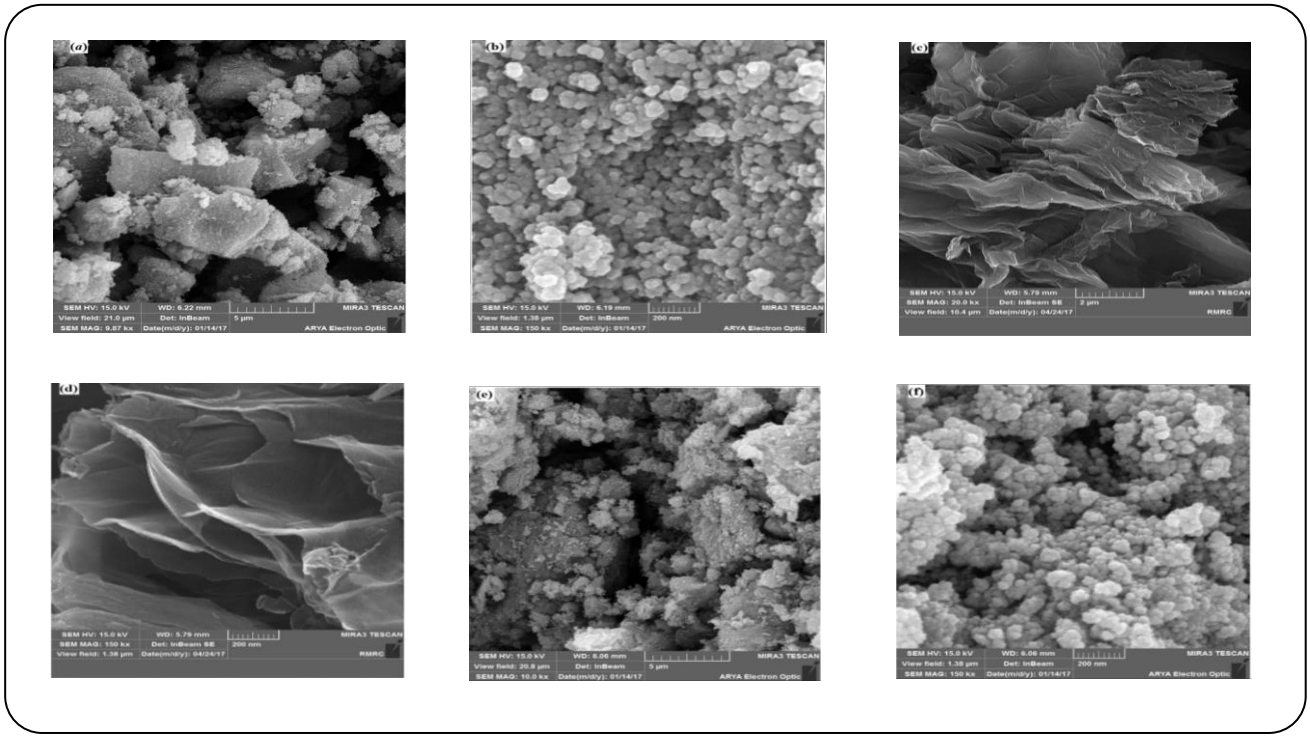

Fig. 4: SEM images of (a, b) Fe_3O_4, (c, d) GO, and (e, f) Fe_3O_4@GO.

to the carbon plane are 1385 and 1640 cm^{-1}, originates from H-O-H bending vibrations in the water molecule. Also, symmetric C-H stretches (CH_3) at 2853 cm^{-1}, asymmetric C-H stretches (CH_2) at 2925 cm^{-1} and asymmetric C-H stretches (CH_3) at 2960 cm^{-1} were detected. The bond at around 2360 and 2360 cm^{-1} is assigned to CO_2 originated from the air during FTIR measurement. Absorption peaks at 1720, 1545, 1052 and 1160 cm^{-1} appear in the FT-IR spectrum of Fe_3O_4@GO confirms that GO has been assembled on the Fe_3O_4.

The morphologies of the pristine Fe_3O_4 nanoparticles, GO and the resulting Fe_3O_4@GO nanoparticles were characterized by SEM shown in Fig. 4. The pristine Fe_3O_4 particles had a narrow size dispersion as shown Figs. 4a, 4b. Figs. 4c, 4d show the typical SEM image of the GO, displaying that the product consists of randomly aggregated, thin and crumpled sheets, showing the flower shape. After designing the assembly of superparamagnetic Fe_3O_4 nanoparticles with GO nanosheets, the superparamagnetic Fe_3O_4@GO

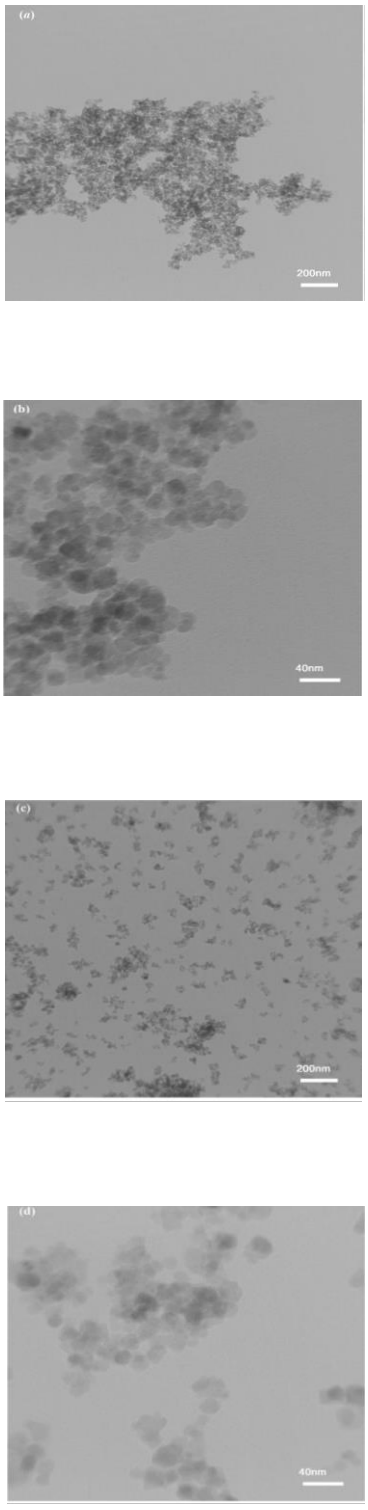

Fig. 5: TEM images of (a, b) Fe_3O_4 and (c, d) Fe_3O_4@GO.

nanoparticles are formed (Figs. 4e, 4f). TEM micrograph of the samples is shown in Figs. 5a, 5b. These images show the nanosized particles smaller than 100 nm that form very dense aggregated Fe_3O_4 nanoparticles. But, the assembly of superparamagnetic Fe_3O_4 nanoparticles with GO nanosheets does not form aggregated Fe_3O_4@GO nanoparticles (Fig. 5c). The Fe_3O_4@GO nanoparticles show crinkled and rough surface textures which may be important for preventing aggregation of graphene and maintaining high surface area with a particular advantage of loading magnetic nanoparticles (Fig. 5d), which can be more clearly observed at the interface between two particles (Fig. 5d). This can be attributed to the presence of a flexible and thin GO shell.

Magnetic Measurements

The S-like magnetization curves of the Fe_3O_4 and Fe_3O_4@GO nanoparticles are shown in Fig. 6. The values of coercivity field (H_C) and remanence magnetization (M_r) are 1.07Oe and 0.054emu/g for Fe_3O_4 and 3.40Oe and 0.199emu/g for Fe_3O_4@GO. The low H_C and M_r of the samples indicate a superparamagnetic behaviour. The increase of H_C after designing the assembly of superparamagnetic Fe_3O_4 nanoparticles with GO nano-sheets can be related to increase of magnetic anisotropy that superparamagnetic behavior of these samples. The saturation magnetizations of the pristine Fe_3O_4 and the Fe_3O_4@GO were 65 and 60 emu/g, respectively. The ~8% decrease in magnetization suggests that the loading of GO and APTMS introduced onto the original Fe_3O_4 nanoparticles was about 8% by weight. However, the ratio of original Fe_3O_4 to GO powder used for preparing of studied sample Fe_3O_4@GO is 15%. The saturation magnetization of Fe_3O_4@GO (60.4 emu/g) is much larger than the value previously reported for a Fe_3O_4@polymer core–shell material [22]. Such as large saturation magnetization should result in a magnetic force which is sufficient for the separation of large biomolecules, allowing it to be used in practical magnetic bioseparation processes [8]. The introduction of the magnetic core into GO nanosheets should make the separation of the resulting carrier material much more rapid and convenient compared with using GO nanosheets alone.

Optical properties

Variation of $(\alpha h\upsilon)^2$ with photon energy $h\upsilon$ for the nanoparticles is shown in Fig. 7. One can observe that

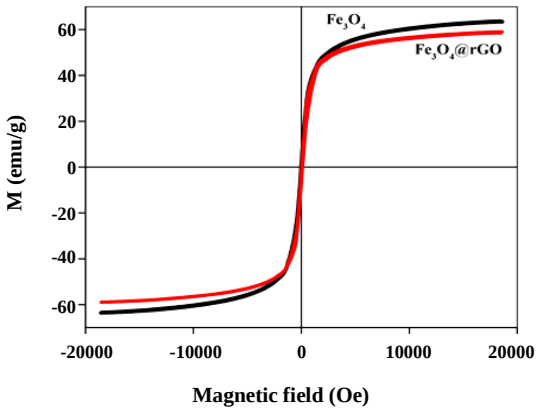

Fig. 6: Magnetization curves of Fe_3O_4 and Fe_3O_4@GO.

the plots are linear over a wide range of photon energy suggesting direct transitions. The direct band gap energies of the nanoparticles were calculated from the intersections of the straight line with the energy axis [18]. The band gap energy of the Fe_3O_4 nanoparticles and GO nanosheets are 2.77 eV and 3.07 eV, respectively. After deigning assembly of Fe_3O_4 with GO, the optical band gap of Fe_3O_4 is reduced to 2.64 eV. The reduction of the band gap energy of Fe_3O_4@GO as compared with Fe_3O_4 nanoparticles cannot be a result of the quantum confinement phenomenon due to the size of the nanoparticle observed in TEM images. This decrease is the result of the effect of the graphene oxide wrapped on the electronic structure of Fe_3O_4.

Photocatalytic Tests

Photocatalytic degradation of MB and MO in the presence of the different catalyst (blank, Fe_3O_4 and Fe_3O_4@GO) at room temperature under natural pH are shown in Figs. 8a, 8b. For all the experiments mentioned here, the MB and MO dye concentration were kept constant to 20mg per 1 liter of water. This was used as stalk solution, out of which 30 ml solution was used for all individual experiments. In this aliquot, 10 mg (500 mg/L) of catalyst was added, and the solution was subjected to ambient sunlight.

The efficiency of photocatalytic degradation of the samples was calculated by the following formula [13]:

$$DC(\%) = \frac{C_o - C_t}{C_o} = \frac{A_o - A_t}{A_o} \quad (4)$$

Where Co (A_o) is the solution concentration (initial absorbance) of MB and MO solution without any

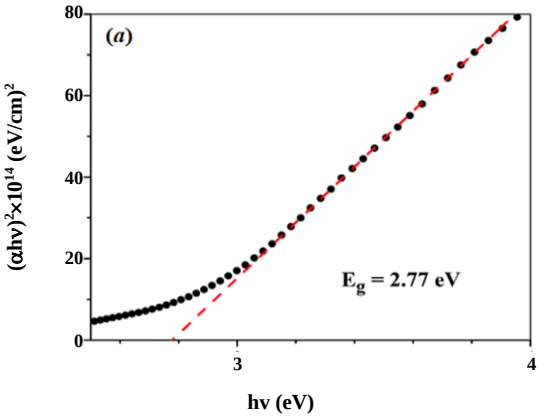

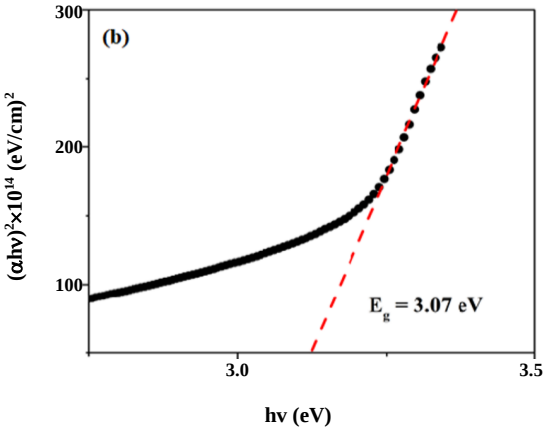

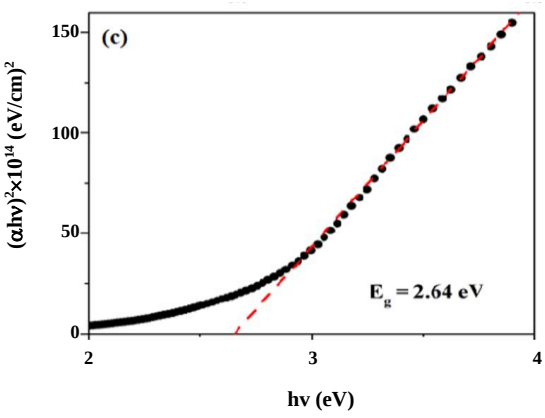

Fig. 7: The plot of the Tauc's equation to obtain band gap of (a) Fe_3O_4, (b) GO, and (c) Fe_3O_4@GO.

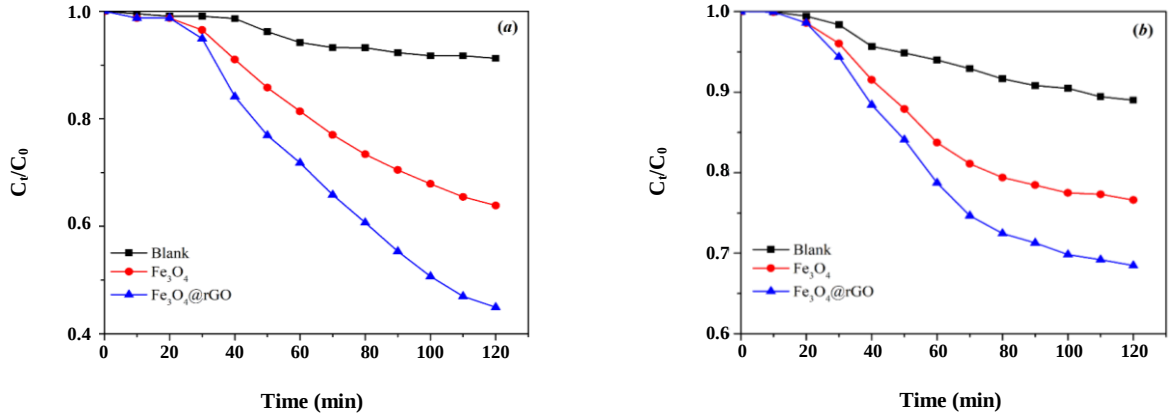

Fig. 8 Photocatalytic degradation of MB and MO in the presence of the different catalyst at room temperature under natural pH (blank, Fe_3O_4 and Fe_3O_4@GO).

exposure before degradation, and Ct (A_t) is the solution concentration (absorbance) of MB and MO after photo-irradiation for time (t). Concentrations of MB and MO were estimated at peak wavelength 607 and 504 nm corresponding to the characteristic absorbance peak (maximum absorption) for MB and MO, respectively, from UV-Vis spectra taken initially and after every ten minutes, irradiation of ambient sunlight [13].

To verify the contributions from different components to the degradation of MB and MO, Fe_3O_4 and Fe_3O_4@GO were chosen to act as the catalysts. It can be obviously seen from the degradation curves in Figs. 8a,8b that Fe_3O_4@GO shows the better degradation performance. The degradation process was low at the beginning up to 20 min in dark medium, but, was quick after 50 min when the samples placed in ambient sunlight. Then, the reaction rate decreased after 50 min. from beginning in sunlight, which can be attributed to the reason that the ferrous ions existed in Fe_3O_4 had been almost totally consumed and the conversion rate of ferric to ferrous is far less than the ferric ions' consumption rate [7]. It can also conclude from Figs. 8a, 8b that when the samples, whose structure and morphology is similar to Fe_3O_4 except for the component, were utilized as the catalysts to decompose MB and MO, their performance is not as efficient as Fe_3O_4@GO. Besides, the ferromagnetic of Fe_3O_4 make the catalysts facilely separable from the solution for subsequent usage. The existence of GO not only endows the catalysts good adsorption of MB and MO which may be beneficial to the degradation of MB and MO, but also endues the catalysts with extended usage of the solar energy.

Also, the photocatalytic tests in Figs. 8a,8b show that the degradation efficiency of MB is higher than MO due to the different chemical structure. According to the previous reports [23], which is an acidic color component, MO is less stable in the acidic environment, and its color change takes place easier from the azo form (Fig. 1). Based on the SCF energy calculations, a chemical structure for pH $\geq$ 4.4 is geometrically more stable and the more stability that can justify optimal pH (pH $\leq$ 3.1) for absorption and catalytic degradation of MO.

The reusability of Fe_3O_4@GO was investigated in four cycles in Fig. 9. Reusability of the catalysts is one of the most important factors which make it as a useful economical catalyst. So, checking the recyclability is an essential test. High photocatalytic activity of Fe_3O_4@GO leads to high recyclability which is demonstrated in Fig. 9. The yield of the product approximately decreases less than 5 percent after four successive cycles due to adsorption of MB and MO on the surface of GO. The decrease in the surface to volume ratio of GO will reduce the photocatalytic activity of the Fe_3O_4@GO. This fact indicates that the possibility of photochemical activity of the catalyst is more than adsorption as result of activated surface.

CONCLUSIONS

In this work, the GO was wrapped on Fe_3O_4 nanospheres by using an electrostatic layer-by-layer method. The resulting Fe_3O_4@GO composites offer

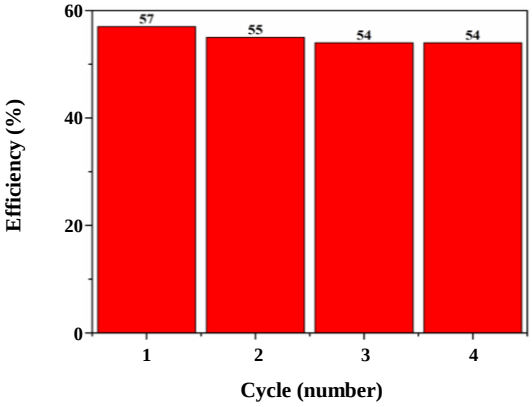

Fig. 9 reusability of Fe_3O_4@GO in photocatalytic degradation of MB.

the combined advantages of Fe_3O_4 (high magnetization and sensitive magnetic response) and GO (good dispersibility in aqueous solution). The experiments of degrading MB and MO confirmed that the obtained catalysts could perform the great catalytic activity even if it was used in the neutral pH and irradiated by visible light. The comparison of the catalytic activity among Fe_3O_4 and Fe_3O_4@GO showed that the two components composed the catalysts possessed synergic effects which may be beneficial to the degradation of the recalcitrant organics.

Received : Aug. 18, 2018 ; Accepted : Jan. 28, 2019

REFERENCES

[1] Gholizadeh A., A Comparative Study of Physical Properties in Fe_3O_4 Nanoparticles Prepared by Coprecipitation and Citrate Methods, *Journal of the American Ceramic Society*, **100**(8): 3577-3588 (2017).

[2] Gholizadeh A., Jafari E., Effects of Sintering Atmosphere and Temperature on Structural and Magnetic Properties of Ni-Cu-Zn ferrite nano-Particles: Magnetic Enhancement by a Reducing Atmosphere, *J. Magn. Magn. Mater.*, **422**: 328–36 (2017).

[3] Gholizadeh A., A Comparative Study of the Physical Properties of Cu-Zn Ferrites Annealed under Different Atmospheres and Temperatures: Magnetic Enhancement of $Cu_{0.5}Zn_{0.5}Fe_2O_4$ Nanoparticles by a Reducing Atmosphere, *Journal of Magnetism and Magnetic Materials*, **452**: 389–397 (2018).

[4] Shamgani N., Gholizadeh A., Structural, Magnetic and Elastic Properties of Mn0.3−xMgxCu0.2Zn0.5Fe3O4 Nanoparticles, *Ceramics International*, **45**: 239–246 (2019).

[5] Pei S., Cheng H.-M., The Reduction of Graphene Oxide, *Carbon*, **50**: 3210–3228 (2012).

[6] Vinayan B.P., Nagar R., Raman V., Rajalakshmi N., Dhathathreyan K.S., Ramaprabhu S., Synthesis of Graphene-Multiwalled Carbon Nanotubes Hybrid Nanostructure by Strengthened Electrostatic Interaction and its Lithium Ion Battery Application, *J. Mater. Chem.*, **22**: 9949 (2012).

[7] Yang X., Chen W., Huang J., Zhou Y., Zhu Y., Li Ch., Rapid Degradation of Methylene Blue in a Novel Heterogeneous Fe_3O_4@rGO@TiO_2-Catalyzed Photo-Fenton System, *Sci. Rep.*, **5**: 10632 (2015).

[8] Wei H., Yang W., Xi Q., Chen X., Preparation of Fe_3O_4@graphene Oxide Core–shell Magnetic Particles for Use in Protein Adsorption, *Materials Letters*, **82**: 224–226 (2012).

[9] Ouyang K., Zhu Ch., Zhao Y., Wang L., Xie Sh., Wang Q., Adsorption Mechanism of Magnetically Separable Fe_3O_4/Graphene Oxide Hybrids, *Applied Surface Science*, **355**: 562–569 (2015).

[10] He F., Fan J., Ma D., Zhang L., Leung Ch., Chan H.L., The Attachment of Fe_3O_4 Nanoparticles to Graphene Oxide by Covalent Bonding, *Carbon*, **48**: 3139 –3144 (2010).

[11] Li Y., Chu J., Qi J., Li X., An Easy and Novel Approach for the Decoration of Graphene Oxide by Fe_3O_4 Nanoparticles, *Applied Surface Science*, **257**: 6059-6062 (2011).

[12] Yu L., Chen J., Liang Zh., Xu W., Chen L., Ye D., Degradation of Phenol Using Fe_3O_4-GO Nanocomposite as a Heterogeneous Photo-Fenton Catalyst, *Separation and Purification Technology*, **171**: 80–87 (2016).

[13] Yousefi H., Gholizadeh A., Mirbeig Sabzevari Z., Malekzadeh A., Structural Features of $La_{0.55}Ca_{0.45}A_{0.50}Co_{0.50}O_3$ (A=Mg, Mn) Nanoparticles Over Photo-Degradation of Methyl Blue, *J. Nanoanalysis*, **4**(4): 324-333 (2017).

[14] Soleimani F., Salehi M., Gholizadeh A., Hydrothermal Synthesis, Structural and Catalytic Studies of $CuBi_2O_4$ Nanoparticles, *J. Nanoanalysis*, **4**(3): 239-246 (2017).

[15] Gholizadeh A., Malekzadeh A, Pourarian F., Rapid And Efficient Synthesis of Reduced Graphene Oxide Nano-Sheets Using CO Ambient Atmosphere as a Reducing Agent, *Journal of Materials Science: Materials in Electronics*, **29**(22): 19402-19412 (2018).

[16] Gholizadeh A., $La_{1-x}Ca_xCo_{1-y}Mg_yO_3$ Nano-Perovskites as CO oxidation catalysts: structural and catalytic properties, *J. Am. Ceram. Soc.*, **100**: 813 (2017).

[17] Mahmoudi S., Gholizadeh A., Effect of Non-Magnetic Ions Substitution on the Structure and Magnetic Properties of $Y_{3-x}Sr_xFe_{5-x}Zr_xO_{12}$ Nanoparticles, *Journal of Magnetism and Magnetic Materials*, **456**: 46–55 (2018).

[18] Gholizadeh A., Tajabor N., Influence of N_2- and Ar-Ambient Annealing on the Physical Properties of SnO_2:Co Transparent Conducting Films, *Mater. Sci. Semicond. Process.*, **13**: 162-166 (2010).

[19] Soleimani F., Salehi M., Ahmad Gholizadeh, Synthesize and Characterization of $Ni_{0.5}Cu_{0.5}Cr_2O_4$ Nanostructure for Discoloration of Aniline Dye under Visible Light from Wastewater, *Iranian Journal of Chemistry and Chemical Engineering (IJCCE)*, **39**(2): 11-19 (2020).

[20] Gholizadeh A., The Effects of A/B-Site Substitution on Structural, Redox and Catalytic Properties of Lanthanum Ferrite Nanoparticles, *Journal of Materials Research and Technology*, https://doi.org/10.1016/j.jmrt.2017.12.006.

[21] Gholizadeh A., Ganjehie S., Ketabi S.A., Microstructure and Swelling Behaviour of Poly (Acrylamide-co-Acrylic Acid) Based Nanocomposite Superabsorbent Hydrogels, *J. Nanoanalysis*, **5**(3): 195-201 (2018).

[22] Luo X, Liu S, Zhou J, Zhang L., In Situ Synthesis of Fe_3O_4/Cellulose Microspheres with Magnetic-Induced Protein Delivery, *J. Mater. Chem.*, **19**: 3538–3545 (2009).

[23] Ghiasi M., Malekzadeh A., Solar Photocatalytic Degradation of Methyl Orange over $La_{0.7}Sr_{0.3}MnO_3$ Nano-Perovskite, *Separation and Purification Technology*, **134**: 12–19 (2014).